Journal of Molecular Liquids xxx (xxxx) 122957

Contents lists available at ScienceDirect

Journal of Molecular Liquids

journal homepage: www.elsevier.com/locate/molliq

Self-assembling of glutathione in aqueous environment: A combined experimental and theoretical study

A. Tryfon [a], P. Siafarika [a], C. Kouderis [a], A.G. Kalampounias [a, b, *]

[a] Department of Chemistry, University of Ioannina, GR-45110 Ioannina, Greece
[b] University Research Center of Ioannina (URCI), Institute of Materials Science and Computing, GR-45110 Ioannina, Greece

ARTICLE INFO

Article history:
Received 7 June 2023
Received in revised form 3 August 2023
Accepted 28 August 2023

Keywords:
Glutathione
Tripeptides
Ultrasonically induced birefringence
Molecular docking
Self-association

ABSTRACT

Detailed concentration-dependent measurements of transient and stationary ultrasonically induced birefringence were combined with molecular docking and DFT techniques to study the formation of glutathione (GSH) self-aggregates in aqueous solutions. Molecular docking revealed the formation of dimers through hydrogen bonding with a binding free energy equal to −3.44 kcal/mol. The behavior of stationary birefringence measurements with concentration allowed us to assign the observed relaxation process to self-association mechanism between glutathione molecules. Systematic analysis of the birefringence traces in the transient region permitted the evaluation of the orientational relaxation times and the corresponding hydrodynamic volumes. Combining the concentration dependent spectroscopic data with supplementary measurements of several physical properties, such as mass density, shear viscosity, sound speed, isentropic compressibility, specific conductivity, and pH, the self-association scheme has been established. The chemical reactivity and the biological activity of the GSH monomer and dimer species were also evaluated and discussed in the context of the fair competence of GSH molecules to interact forming aggregates in aqueous environment.

1. Introduction

Glutathione (GSH) is a tripeptide comprised of three amino acids, glutamic acid, cysteine, and glycine, with a γ-peptide bond between the amino group of the cysteine and carboxyl of the glutamic acid [1]. GSH is the most abundant non-protein thiol in mammalian and plant cells at concentrations up to 0.01 M [2]. It is mainly found in the cellular cytoplasm, while a smaller portion of it is located into the nucleus, mitochondria, and endoplasmic reticulum [3]. Furthermore, GSH is present in certain organs and tissues, such as liver, pancreas, spleen, and kidneys [4]. Glutathione exists in cells in two states, the reduced (GSH) and the oxidized (GSSG) one. Oxidized glutathione is formed when two GSH molecules are linked covalently via a disulfide bond. Under oxidative stress, GSH is converted to GSSG either chemically or enzymatically. This disulfide can reversely be reduced to GSH by the actions of an enzyme named glutathione reductase [1,3].

This low-molecular-weight peptide is involved in a variety of vital intercellular reactions. Firstly, GSH acts as an antioxidant by directly scavenging free radicals and other reactive oxygen species (ROS), through enzymatic reactions that oxidize GSH to GSSG. Notably, GSH detoxifies xenobiotics and electrophilic compounds through a process known as conjugation, facilitating their metabolism [5]. Finally, GSH protects thiols and regulates redox reactions that cellular thiol proteins are involved in and is required for prostaglandin and leukotriene biosynthesis [6]. Reactive oxygen species generated by antibiotic treatment are known to induce cell death. Cells can exhibit antibiotic resistance through enzymatic modification, exclusion, export, and modulation of nuclear signaling pathways. Glutathione's presence in cells can reduce ROS levels, promote excretion from the body through glutathione-S-transferase's actions, and regulate antibiotic sensitivity in non-photosynthetic organisms [7,8].

In medicine, glutathione's antioxidant abilities are used in several life-threatening diseases, such as liver disease, cystic fibrosis, and aging process. In addition, GSH deficiency may also be associated with neurodegenerative disorders, cardiovascular diseases, immune diseases, and chronic age-related diseases [9]. Glutathione is also widely used in food industry, where its main role is to extend food storage period, inhibit browning, and increase flavor [10].

When applying an acoustic field in an isotropic liquid or solution that is in equilibrium state, the ultrasound wave will force the molecules to orient in the direction of the field axis and the system becomes birefringent. In other words, the system acts as anisotropic with its optical axis parallel to the direction of the sound propagation. The birefringence phenomenon is triggered by the sinusoidal velocity gradient and by the radiation pressure of the ultrasound [11,12]. By probing the acoustically induced birefringence, we gain information about the opti-

* Corresponding author at: Department of Chemistry, University of Ioannina, GR-45110 Ioannina, Greece.
E-mail address: akalamp@uoi.gr (A.G. Kalampounias).

https://doi.org/10.1016/j.molliq.2023.122957
0167-7322/© 20XX

cal and acoustical properties of the molecules [13]. Birefringence measurements are exceptionally sensitive to solution state conformations and may provide geometrical characterization of the particles. The ability to control the orientation of molecules that possess significant antioxidant abilities could open new possibilities of particle trap applications [14–16] and thus, the method of particle manipulation in solutions by applying a low-intensity and low-frequency acoustic field is of crucial importance.

The purpose of the present paper is to understand the birefringence phenomenon of aqueous glutathione solutions. Concentration-dependent birefringence are used to study the dynamic response of the system. Moreover, supplementary measurements of several physical properties, such as density, viscosity, conductivity, and pH were also performed. Molecular docking was employed to determine the possibility of self-aggregation, and the volume change due to the self-association of GSH was estimated by means of MP6 semi-empirical method and compared with the experimental findings. The chemical reactivity and the biological activity of the GSH monomer and dimer species were evaluated and compared.

2. Materials and methods

2.1. Materials

Crystalline reduced glutathione in the form of powder (Merck, purity >99%, CAS # 70-18-8) was weighed and dissolved in triply distilled water without any further purification. The IUPAC name of glutathione is γ-Glutamylcysteinylglycine or (2S)-2-Amino-5-({(2R)-1-[(carboxymethyl)amino]-1-oxo-3-sulfanylpropan-2-yl}amino)-5-oxopentanoic acid. Complete dissolution of the solid was achieved under continuous stirring at ambient temperature and pressure conditions. The so obtained solutions were colorless and without any solid residual. All measurements were performed only in fresh solutions to avoid unwanted implications due to potential degradation of GSH. Glutahione is stable as a powder for up to 5 years at 4 °C, but it is very unstable when it is solubilized in aqueous solutions. After resuspending in an aqueous solution, immediate freezing at −20 °C is required [17]. Aqueous solutions readily oxidize in air and reduced glutathione (GSH) becomes oxidized to its disulfide forming the oxidized glutathione (GSSG). Seven solutions of GSH were prepared at concentrations 1, 2, 3, 4, 5, 7.5, and 10 mM.

2.2. Acoustically induced birefringence setup

The experimental setup of the acoustically induced birefringence technique is presented in Fig. 1. A detailed description can be found in [18 and references therein]. A cylindrical cell made of fused silica with a fixed optical path length of 1 cm was used for all measurements. The temperature of the cell was kept constant within ±0.01 °C. The cell was properly sealed to avoid any directional flow of the liquid that could affect the accuracy of the measurements. At the one phase of the cell a piezoelectric element (Olympus, V111) was attached to the one parallel phase of the cylindrical cell ensuring perfect contact, which is crucial to achieve maximum transmission of the acoustic wave. Some sort of couplant has been used between the transducer and the sample to ensure proper transmission of the generated pulse. In our case, common medical ultrasound gel was used. This way the transducer is in perfect contact with the one face of the optical cell. A pulse generator (TTi, TGP3151) was used to trigger with a squared electric pulse in the low-MHz region a wide band piezoelectric element (Olympus, f = 1 MHz). The repetition rate and the number of the cycles were carefully selected to avoid unwanted ultrasonic heating and streaming.

A linearly polarized He-Ne laser (Melles Griot, 5mW, λ = 632.8 nm) was used a probe for the birefringence measurements. The laser beam, at an angle of polarization set at 45°, passes through a polarizer and then through the sample container in a direction perpendicular to the propagation of the acoustic wave. After the cell, the beam passes through a quarter-wave plate and an analyzer and finally reaches a fast and sensitive photodiode. Information concerning the ultrasonic intensity can be obtained indirectly by measuring the light intensity emerging from the liquid. All signals were monitored in a digital oscilloscope (Tektronix, TBS 1201B-EDU), averaged after 256 runs and saved in a computer for further analysis. Special attention has been paid to select the acoustic frequency in the experiment taking into account the mechanical resonances of the container. The vibration frequencies observed on the container's surface will depend on the material and geometry of the cell, the physical properties of the fluid filling the container and the corresponding volume of the liquid in the cell. In general, the mathematical model dealing with the mechanical resonances of the container is a rather complex problem. Two different phenomena have to be taken into account, namely the vibration of the container filled with fluid and the container filled with air (empty cell).

2.3. Additional physical properties

The sound velocity in the GSH aqueous solutions were determined by means of the pulse-echo overlap method. The experimental error was estimated to be less than ±0.01%. A detailed description of the pulse-echo overlap method could be found in references [19–21].

Mass density measurements were carried out utilizing a thermostated density meter (Anton Paar, DMA 40) with an accuracy of ±0.0001 gr/cm³. Liquid density can be measured using the DMA 40 digital densitometer, which consists of a U-shaped tube horizontally immersed in a water-filled chamber. The temperature of the chamber can be controlled by connecting the densitometer to a constant temperature circulator water bath. To calculate the liquid density, it is necessary to

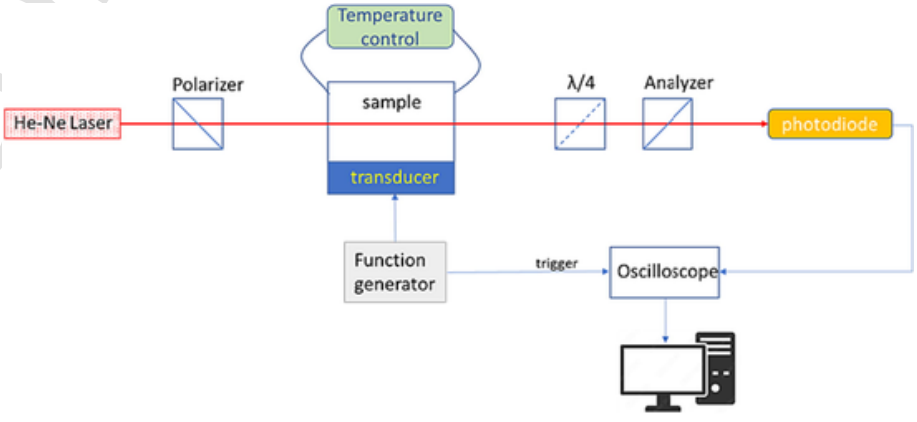

Fig. 1. Experimental setup for ultrasonically induced birefringence measurements.

calibrate the densitometer with air and distilled water. The densitometer does not show the density directly; instead, it displays the "weight" of the tube filled with the fluid of interest.

Kinematic viscosity coefficient was measured by means of an Ubbelohde-type digital viscosity meter (Schott, ViscoSystem AVS series) with an accuracy of 1%. Viscosity measurements were thermostated at the desired temperature using a water circulator. From the kinematic viscosity and density values, the shear or dynamic viscosity can be easily determined. In the case of the Ubbelohde viscometers, the transition point from the capillary to the levelling bulb has the shape of a ball joint being the end point of an additional venting tube. After filling the sample through the tube into the container, the venting tube is closed. Depending on the operational mode, i.e. pressing or sucking action, the sample is filled by over-pressure applied to tube or by suction via the tube into the reference level vessel, the capillaries, the measuring sphere, and at least up to half of the pre-run sphere. After venting tube, the liquid column in the levelling bulb breaks off. At the exit of the capillary the so-called suspended level develops. For this reason, only a limited sample quantity - max., min. filling marks - may be filled in. After ventilating tube, the sample flowing out of the capillary will flow off along the inner wall of the levelling bulb in the form of a film. In this way the hydrostatic pressure of the liquid column is independent of the sample quantity being filled in. In addition, owing to the geometrical shaping of the levelling bulb, the influence of surface tension on the measurement result is almost eliminated. In the case of the Ubbelohde viscometer, the measurement is aimed at the time required by the liquid meniscus to sink between two successive annular measurement marks.

Specific conductivity was evaluated utilizing a conductivity meter (Orion Research, 101) at the desired temperature. The constant of the electrode was equal to 1. The error in specific conductivity was less than 1%. The ORION Model 101 allows selection of three AC (3 kHz, 1 kHz, 80 Hz) permitting a choice of cell types. It consists of an oscillator, amplifier, and synchronous detector. The DC output is proportional to cell conductance, with minimum interference from capacitance because of the synchronous detector. This electronic design permits the use of any electrically conducting material for electrode construction, the only limitations being corrosion by the solution to be measured.

A pH-meter (Crison, micropH 2002) was used to determine pH of each solution at a constant temperature of 20 °C. The instrument has a U-type glass electrode that enables measurements in a range 0 to 14 and temperatures from 20 to 80 °C. Potassium chloride (KCl) solution corresponding to concentration 3 M was used as reference electrolyte. The resolution in the pH measurement is 0.01. The instrument was calibrated using buffer solutions with pH 4 and 7.02 before measurements. The accuracy of the values was ±0.03 units.

2.4. Molecular docking

A 3D model of glutathione was fetched from PubChem (PubChem CID: 124886). Prior to molecular docking calculations, the structure of glutathione was optimized, and its molecular volume was estimated using PM6 semiempirical method. Molecular docking analysis was performed using Auto Dock Tools (ADT) and Auto Dock, version 4.2, aiming to elucidate the presence of potential self-aggregation between glutathione monomers, as before [22]. Initially, the size of the box was set at 25 Å × 25 Å × 25 Å that was large enough to accommodate both the host and the guest molecules. For each docking computation, the assignment of the partial charges was done by implementing Gasteiger charges. The number of initial poses was set at 5000. A grid-based energy-computation method was used for the calculation of the free binding energy and with the help of the Lamarckian genetic algorithm the most plausible docking pose was estimated [23].

2.5. Quantum-mechanical calculations

The monomer and dimer structures of glutathione were used as input to perform the quantum–mechanical calculations. The so-called B3-LYP hybrid exchange–correlation functional [24,25] combined with the 6-31G(d,p) split-valence basis set were used to predict the HOMO and LUMO orbitals and calculate their energy gap. The B3 functional, in fact, contains a linear combination of exact hybrid form exchange, Slater exchange and Becke gradient corrected exchange. The functional used in the description of the studied molecular system has been proved its validity in calculating the HOMO and LUMO energies and it is a suitable for studying the geometry optimization for the organic molecular system. All theoretical calculations were carried out with the use of the Gaussian 09 series of programs in a vacuum environment without any interactions with the solvent and tight optimization convergence criteria.

3. Results and discussion

3.1. Dynamic and structural processes in GSH aqueous solutions

Reduced glutathione (GSH) is responsible for the delivery of various metal ions to a protein which together with a prosthetic group forms a particular biochemical molecule such as a hormone or enzyme. This property is due to the characteristic molecular structure of GSH, which possesses a variety of biological donor atoms and to its conformations and the inherent flexibility of the molecule. In Fig. 2 is presented the structure of the reduced glutathione, where eight coordination sites are observed, namely two carboxyls, one amino, two carbonyls, two amide and one thiol groups. The two pairs of carbonyls and amides constitute the two peptide bonds. Under oxidized conditions, all these donor

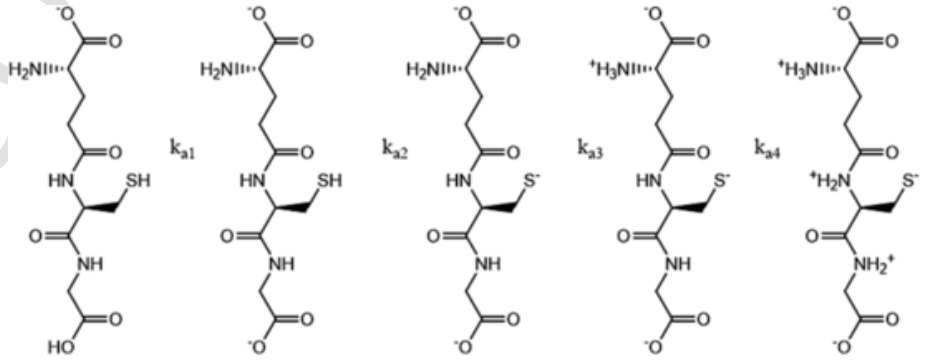

Fig. 2. The structure of the reduced glutathione. These are the possible tautomers of glutathione present in aqueous solutions in various pH. Tautomers differ from each other by a dissociation step and the corresponding dissociation constants are k_{a1} = 2.38, ka_2 = 3.70, k_{a3} = 8.61 and k_{a4} = 9.43, respectively. The population of each tautomer is strongly dependent on the pH of the solution.

groups are doubled apart from thiols that are replaced by a disulfide bond. Upon dissolution of GSH in water several protonation processes occur including the deprotonation of the two carboxylic acids, and the thiol group and the protonation of amine.

Concerning the possible conformational of glutathione, it was proposed that at neutral pH, the most abundant conformation is that with the amine and carboxylate of the Glutamic acid (Glu) residue separated from the thiol group at the maximum degree. Thiol group is in trans configuration relative to each one of the two peptide bonds that are flank the Cysteine (Cys) residue [26,27]. The equilibrium between different GSH conformers may be presented as:

$$GSH \leftrightarrows (GSH)^{*} \tag{1}$$

where (GSH)* denotes a possible conformer of glutathione.

From the molecular structure of glutathione presented in Fig. 2, it seems that the specific structure may also demonstrate a molecular self-aggregation reaction except proton-transfer and conformational changes. In the low-concentration region, the self-aggregation mean mechanism may be described as:

$$nGSH \leftrightarrows (GSH)_n \tag{2}$$

where *GSH* and $(GSH)_n$ represent the monomer and the aggregate, respectively and n is the aggregation number. The above reaction assumes the possibly stepwise aggregation process as a mean mechanism. This assumption will be reasonable for low aggregation numbers. In the intermediate-concentration region, the interactions between water and GSH molecules are enhanced and mixed aggregates between water and GSH molecules may be formed. This association scheme is represented as:

$$(H_2O)_m + GSH \leftrightarrows GSH \bullet (H_2O)_m \tag{3}$$

The water aggregate and the mixed water-GSH aggregate are denoted as $(H_2O)_m$ and $GSH(H_2O)_m$, respectively in Eq. (3).

It is already reported in the past [3] that glutathione (GSH) is converted to oxidized glutathione (GSSG) by forming a disulfide bond (S-S), only after undergoing an oxidative stress, either intracellularly or chemically. Although this reaction is bidirectional, the enzyme glutathione reductase must be used to convert back GSSG to GSH. The molecular docking calculations performed in this work, revealed that the two S atoms belonging to the two GSH monomers, are at a great distance from each other and the forming dimer is mainly formed by hydrogen bonds. Furthermore, the $(H_2O)_m$ water aggregate and the $GSH(H_2O)_m$ mixed water-GSH aggregate are also formed by hydrogen-bonding. In Fig. 3 are shown the molecular structures of the monomer and dimer, respectively. The structure of the GSH molecule is subjected to optimization procedure before uses as input in the molecular docking study. The output of the molecular docking study is the structure of the GSH dimer that is presented in the right part of Fig. 3. The bonds between the two monomeric units constituting the formed dimer, are clearly denoted and it seems that the interactions are mostly hydrogen bonds. Specifically, the hydroxyl group of the glutamic acid of the one monomer forms two hydrogen bonds with the other monomer. One bond with the oxygen atom of the glutamic acid and one bond with the hydrogen atom of the sulfur group of cysteine. The hydroxyl group of the glutamic acid of the one monomer also forms a hydrogen bond with the oxygen of the cysteine of the other monomer. Furthermore, the oxygen atom of the glutamic acid of the one monomer forms a hydrogen bond with the hydroxyl group of the glycine of the other monomer. The self-aggregation reaction proposed in Fig. 3 corresponds to aggregation number equal to n = 2 and the corresponding binding free energy was estimated equal to −3.44 kcal/mol. The formation of aggregates with higher aggregation number that n = 2, such as trimers, tetramers, etc. is not excluded. Nevertheless, such complicated structures are not expected to occur in the highly dilute region of concentration studied in this work. The oxidation of GSH to GSSG is the basis of all major intercellular reactions involving GSH. However, this phenomenon cannot be observed in aqueous solutions unless an oxidizing agent is present.

3.2. Concentration effect on the physical properties of GSH aqueous solutions

The concentration behavior of mass density and shear viscosity is presented in Fig. 4 (a) and (b), respectively. These physical properties are quite sensitive to alterations in the structure of GSH in aqueous environment. Despite its experimental simplicity, density measurements can be used effectively in the understanding of the concentration-induced changes in the GSH structure. Modifications in the coordination number and in the cross-linking of interstitial spaces imply a transformation from a loose to a compact structure and conversely. All these alterations are reflected in the variation of density with solution concentration. As is observed in Fig. 4 (a), the mass density increases monotonically with concentration implying the transition to a denser packing of the structural units in the network. The variations are almost linear as denoted from the Pearson's coefficient that was estimated equal to r = 0.96191 and can be explained considering changes in the volume of the building blocks constituting the structure. On the other

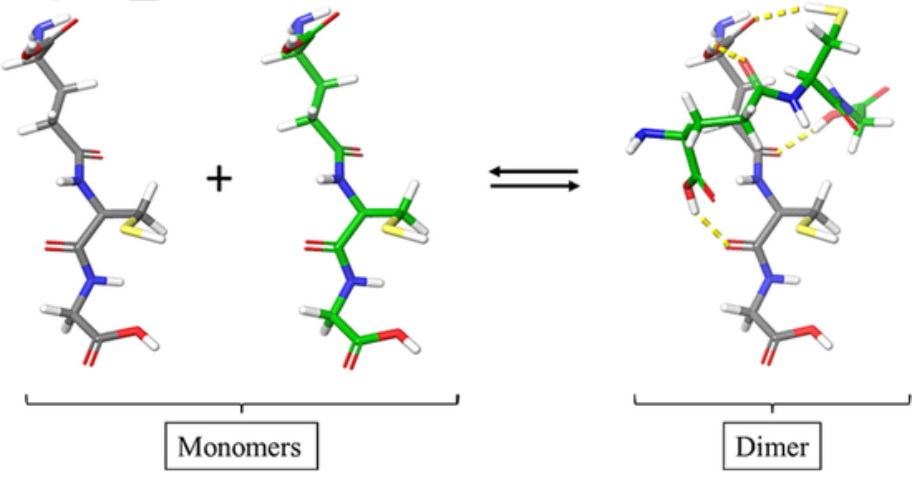

Fig. 3. (Left) The optimized molecular structure of glutathione. (Right) The self-association scheme as received from the molecular docking investigation. See experimental section for more details concerning the computational procedures used. The two monomers, the one on the left with grey carbon atoms (host) and the one with green carbon atoms (guest) were docked forming the dimer.

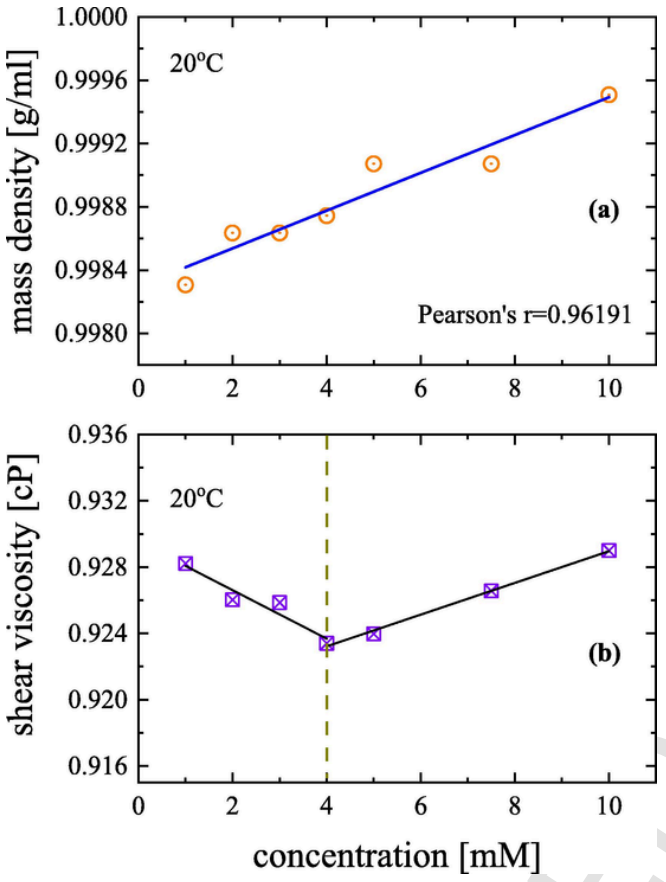

Fig. 4. Mass density (a) and shear viscosity (b) of the aqueous glutathione solutions in the low-concentration region.

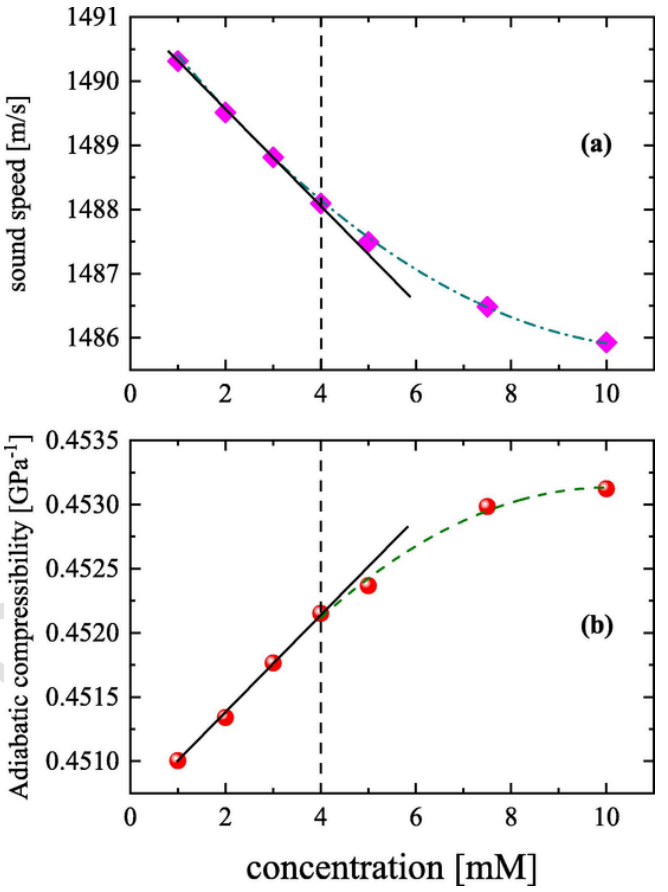

Fig. 5. Sound velocity (a) and adiabatic compressibility (b) of the aqueous glutathione solutions in the low-concentration region.

hand, shear viscosity exhibits an unusual feature below and above 4 mM. The minimum observed in the shear viscosity plot with concentration, as presented in Fig. 4 (b), is similarly related to intermolecular association between GSH molecules in these solutions, since the presence of hydrogen bonding interactions could lead to an analogous variation in shear viscosity. The formation of these hydrogen bonds is confirmed by the molecular docking analysis described in previous section.

The ultrasonic sound speed and the adiabatic compressibility are presented in Fig. 5 (a) and (b), respectively. The variation of the sound speed implies that severe structural alterations occur in the system and that this parameter can be used as a probe for the dynamic response of the system. In the solution, sound consists of compression waves. The hydrogen bonding between GSH molecules perturbates the sound waves inducing a volume change in the basic structural units and consecutively a compressional relaxation. The longitudinal ultrasonic wave is associated with compression and decompression in the direction of the sound propagation. The speed of the compression wave in the fluid is determined by the medium's compressibility and density. The adiabatic compressibility is estimated as:

$$\kappa_s = \left(\rho \bullet u_s^2\right)^{-1} \tag{4}$$

where ρ is the mass density and u_s is the velocity of the ultrasonic wave in the solution. The degree of compressibility of a fluid has strong implications for its dynamics. Most notably, the propagation of sound is dependent on the compressibility of the medium. For solution concentrations up to 4 mM, the behavior of both physical properties is linear, although with negative and positive slopes, while above this concentration the trend alters significantly. The sound speed and the isentropic compressibility reveal a sudden change near 4 mM as the mass density and shear viscosity presented in Fig. 4 (a) and (b), respectively. Despite the different trend of the sound velocity and adiabatic compressibility with concentration, the monotonous variation observed in Fig. 5 in the low-concentration region is indicative of the gradual aggregation process occurring in the aqueous GSH solutions.

In Fig. 6 (a) and (b), are shown the pH and specific conductivity measurements of the aqueous GSH solutions. It is widely accepted that pH is a common factor, which is strongly affecting protein aggregation due to its effects on the zeta potentials and structures of proteins [28, 29]. When pH values are away from the isoelectric point of the protein, its net charge increases, which in turn enhances the electrostatic interaction among protein molecules and affects their aggregation tendency in aqueous environment. Furthermore, pH values other than isoelectric point, can also unfold the structure of the protein and enhance protein aggregation [30]. Even though GSH is by far simpler from structural point of view when compared with a protein, it is important to elucidate the role of pH in GSH self-aggregation at the molecular level. The isoelectric point of the GSH was reported near ~6.5 [31]. The pH values presented in Fig. 6 (a) exhibit an increasing deviation from the isoelectric point indicating the self-aggregation tendency of glutathione with increasing solution concentration. The specific conductivity of the GSH solutions may also progress on the comprehensive understanding of the association mechanism. The specific conductivities of GSH solutions were measured and the results are reported in Fig. 6 (b). The variation of the specific conductivity with concentration reveals a typical for aggregation mechanism behavior. The measured conductivity values were linearly fitted below and above the 4 mM cross point. The Pearson's coefficients for the two regions imply a strong linear correlation.

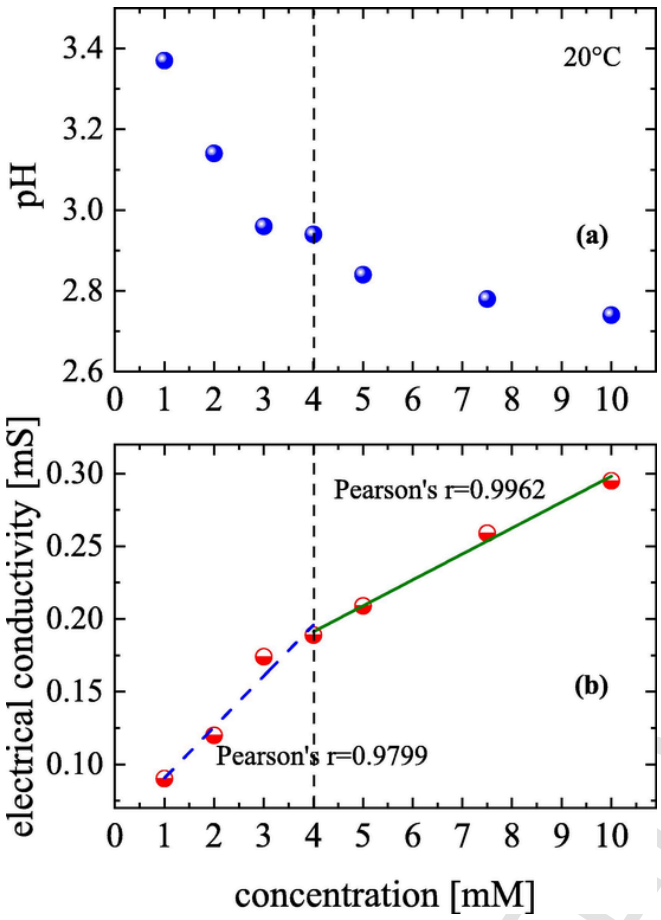

Fig. 6. pH (a) and specific conductivity (b) versus solution concentration. Solid lines represent linear fittings.

3.3. Ultrasonically induced optical birefringence measurements

A representative ultrasonically induced birefringence signal corresponding to a solution with concentration C = 1 mM at 20 °C is shown in Fig. 7 (a). The frequency of the applied square ultrasonic wave was set constant at 753 kHz. The applied ultrasonic pulse is also shown in Fig. 7 (b) for comparison. The birefringence trace is separated into two distinct regions, namely the transient and the stationary or static region. The transient region is characterized by the rise and fall of the birefringence signal, which are attributed to the orientation and disorientation of the system species along the direction of the ultrasonic wave propagation. The orientation and disorientation relaxation mechanisms are not necessarily characterized by the same relaxation times, since the orientation process is a forced process, while the disorientation process is spontaneous. Birefringence signal exhibits a saturation when all the species are fully aligned defining the static or stationary region. The width of the applied ultrasonic pulse was set to fully orient all species and the measured birefringence to reach a constant value. After the perturbation by the squared ultrasonic pulse, the system experiences two difference relaxations, the forward relaxation in the field on and the reverse relaxation in the field off region. After shutting down the acoustic field and the passage of a large amount of time, the system becomes again fully isotropic without any kind of birefringence hysteresis.

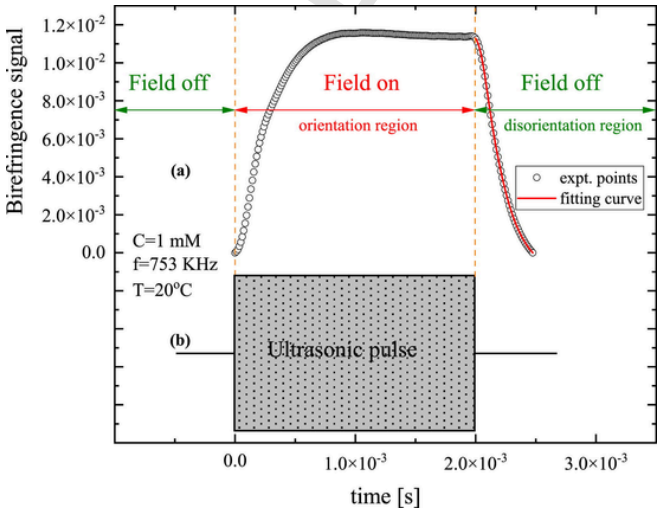

Fig. 7. (a) Representative birefringence signal of a glutathione aqueous solution corresponding to concentration C = 1 mM at 20 °C. The frequency of the applied ultrasonic wave was 753 kHz. (b) The applied ultrasonic pulse.

The variation in the transmitted light intensity has the following general form [32]:

$$\frac{I_\delta(t) - I_a}{I_a} = \frac{\sin^2\left(a + \frac{\delta}{2}\right) - \sin^2 a}{\sin^2 a} \tag{5}$$

I_α corresponds to the light intensity that reaches the photodiode in the absence of the acoustic field, namely the field off region. In this case, the analyzer is set at an angle α relative to the crossed configuration. The phase retardation is related with the observed birefringence according to the equation:

$$\Delta n(t) = \frac{\lambda}{2\pi d}\delta(t) \tag{6}$$

where $\Delta n(t) = n_{//} - n\perp$ denotes the ultrasonically induced change in the refractive index, λ is the laser wavelength and d is the pathlength of the acousto-optical cell.

The rise and the decay times of the birefringence signal both can be fitted to a multiple exponential function. For the birefringence rise, the equation is [33–35]:

$$\Delta n = \sum_{i=1}^{k} \Delta n_{\max,i}(1 - e^{-t/\tau_i}) \tag{7}$$

while for the birefringence decay the signal is given by:

$$\Delta n = \sum_{i=1}^{k} \Delta n_{\max,i} e^{-t/\tau_i} \tag{8}$$

For the discrete distribution of relaxation times, with $\Delta n_{max,i}$ is denoted the contribution of the i-th species to the birefringence at time t = 0. The time τ_i represents the relaxation time of the i-th species. The average relaxation time is related with the area bounded by the normalized rise and decay curve, respectively and the time-axis [8]:

$$\bar{\tau} = \int_0^\infty \frac{\Delta n(t)}{\Delta n_{\max}} dt \tag{9}$$

In Fig. 8 are shown the birefringence values Δn_{max} in the static region as a function of solution concentration at 20 °C. One would expect a rather monotonic trend with increasing concentration. Nevertheless, the Δn_{max} values experience a drastic change when approaching the concentration C = 4 mM. Birefringence seems to follow an almost perfect linear dependency below and above this concentration, although with negative and positive slopes, respectively. The values of Pearson's coefficient below and above 4 mM were estimated equal to −0.99915 and 0.99259 revealing the strong linear dependency. This behavior is

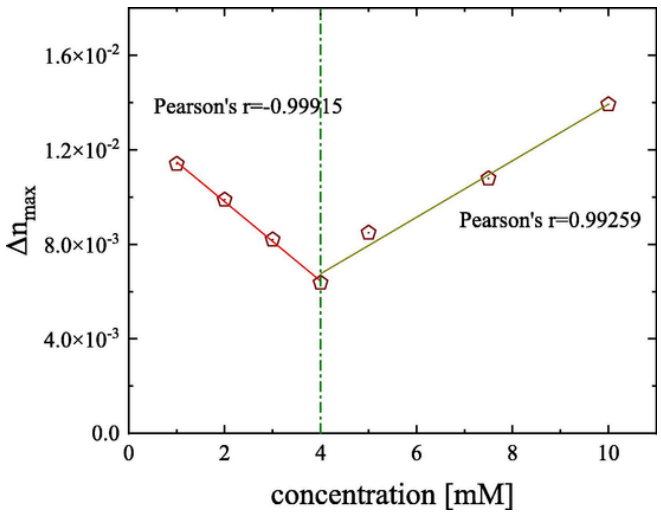

Fig. 8. Maximum birefringence values in the static region as a function of solution concentration at 20 °C. The frequency of the applied ultrasonic wave was kept constant at 753 kHz for all measurements. The values of Pearson's coefficient below and above 4 mM indicate an almost perfect linear dependency.

related with the self-aggregation process occurring in the aqueous GSH solutions forming the dimeric species presented in Fig. 3.

In the field off region, the birefringence signal exhibits an exponential behavior as is shown in Fig. 7. We will focus our analysis on this region since the corresponding relaxation corresponds to a spontaneous disorientation diffusion process. The characteristic relaxation times attributed to this spontaneous process have been determined by fitting the experimental birefringence traces with the Eq. (8). The so obtained results are presented in Fig. 9 for all solution concentrations studied. The disorientation relaxation times follow a linear increase with a Pearson's parameter equal to r = 0.99331. The increase is further enhanced above 4 mM and up to 10 mM, which is the highest concentration studied here. This change is also in this case related with the dimerization reaction of GSH molecules and it seems that the disorientation relaxation times become slower at higher concentrations implying that the population of dimers increases continuously with concentration. The formation of more complicated aggregates, such as trimers, tetramers, etc. are expected to occur at even higher concentrations. The relatively slow relaxation time values presented in Fig. 9 for the disorientation process are indicative of a collective molecular motion over long range.

The experimental relative molecular volume change as a function of concentration for GSH aqueous solutions is presented in Fig. 10. The results reveal that the aggregation induced volume change is strongly influenced by the concentration of the solution. The contribution of potential conformational changes would be much lower compared with the volume change associated with the self-aggregation mechanism, which has a much stronger impact on the overall structure, since greater structural variation would lead to larger molecular volume changes. In Fig. 10, are also shown as open symbols the corresponding theoretically predicted volume change for aggregation number n = 2. The structure of the monomer and dimer were both optimized and then used as input for the volume estimation by means of the PM6 semi-empirical method. The hydrodynamic volume was estimated from the birefringence trace in the field off region. After shutting down the acoustic field, the birefringence decay signal tends to zero due to Brownian rotation/thermal orientational fluctuations of the system particles. The attributed relaxation time is correlated with the hydrodynamic volume through the equation [36]:

$$\tau = \left(\frac{\eta}{k_B T}\right) V_h \tag{10}$$

where η, T and k_B are the shear viscosity of the solvent, the absolute temperature and the Boltzmann's constant, respectively. The ratio final/initial volume was found experimentally equal to 1.62 for concentration 10 mM. The corresponding theoretically calculated ratio between dimer's and monomer's volume was equal 1.95. It seems that dimers dominate the structure of GSH aqueous solutions in the relatively dilute region. The deviation between the two values can be understood if we consider that the molecular docking and MP6 semi-empirical methods were performed in a vacuum environment. The rate of the increase presented in Fig. 10 is different below and above 4 mM, which is probably related with an enhancement of the dimerization process between GSH molecules.

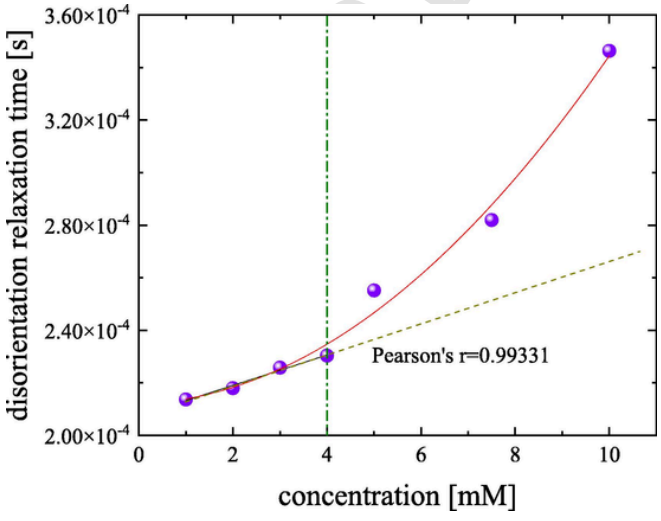

Fig. 9. Characteristic relaxation times in the disorientation region as a function of solution concentration at 20 °C. A linear dependency is observed for concentrations up to 4 mM. Solid line corresponds to 2nd degree polynomial fitting. See text for details concerning the fitting procedure performed for the estimation of the relaxation times.

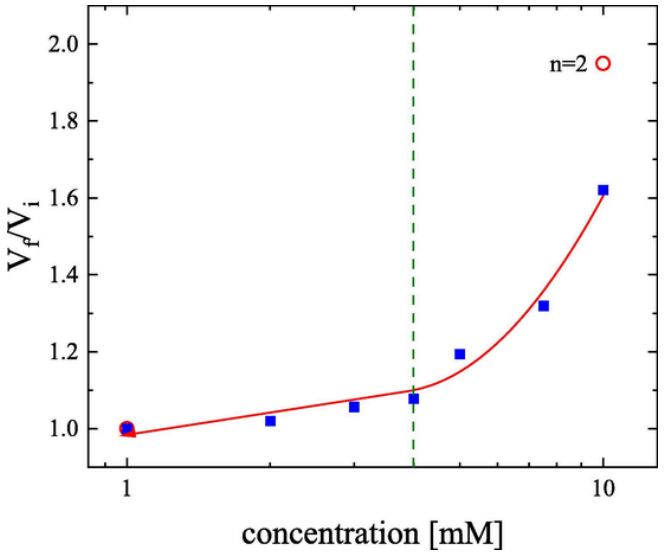

Fig. 10. Experimental relative molecular volume change (final volume/initial volume) as a function of concentration for GSH aqueous solutions (squares). The open circles correspond to the theoretically predicted volume change for aggregation number n = 2.

3.4. Bioactivity scores and quantum global chemical reactivity descriptors

To evaluate several important molecular properties of GSH monomer and dimer, we employed the web-based tool Molinspiration (https://www.molinspiration.com). These properties are linked to the concept of potential drug activity and associated with the relevant criteria of oral bioavailability [37,38]. In Table 1 are shown the calculated molecular properties of GSH monomer and dimer species.

The logP parameter, namely, the log10 value of P, is a constant. It is negative for hydrophilic compounds with higher affinity for the aqueous phase, positive for lipophilic compounds with higher affinity for the lipid/organic solvent phase, and zero for compounds which partition equally between lipid and aqueous phases. logP should have a value lower than 5 for good oral and intestinal absorption. For drugs targeting at central nervous system (CNS) that can cross the blood–brain barrier, the values of logP should be near ~2. For drugs that are developed for sub-lingual absorption, the values of logP value must be higher than 5 [37,38]. logP bioactivity score can be used not only for the estimation of how effectively a drug is adequate for absorption, transportation, and distribution in the human body, but also indicates how this substance should be formulated and dosed [37, 38 and references therein].

On the other hand, parameter milogP is a method for logP prediction developed at Molinspiration software and is based on group contributions that have been obtained by fitting calculated logP with experimental logP for a training set. The training set consists of more than twelve thousand molecules that are used as drugs. Following this methodology, the hydrophobicity values have been received for 35 small simple "basic" fragments and for 185 larger fragments. This way, the intramolecular hydrogen bonding and charge interactions have been taken into account in the calculation of logP. This methodology implemented in Molinspiration software provides a robust calculation for the logP parameter for a great variety of organic and organometallic molecules.

Parameter TPSA, namely the topological polar surface area of a molecule defines the surface sum over all polar atoms or molecules, primarily oxygen and nitrogen, also including their attached hydrogen atoms. The higher the TPSA parameter, the more difficult is for a molecule to permeate cell membranes. High PSA values are indicative of high polarizability or equivalently increased induction interactions between dipoles and/or dipole-induced dipoles since permanent dipoles may induce a temporary dipole in an adjacent molecule.

From milogP values presented in Table 1, it seems that dimers are more hydrophylic relative to GSH monomers, while TPSA values reveal that both GSH monomer and dimer species are not able to permeate cell membranes. Furthermore, the ratio between dimer's and monomer's volume is equal to 2.02, which is close to the 1.95 value calculated by means of MP6 semi-empirical method.

Bioactivity of a molecule, in terms of bioactivity scores, is indicative of the potential pharmaceutical activity of the specific molecule. The same software was used for the on-line calculation of the bioactivity scores which indicate a measure of the ability of the potential drug to interact with the different receptors, namely, to act as G protein-coupled receptors (GPCR ligands), as kinase inhibitors, as ion channel modulators, or to perform interactions with enzymes and nuclear receptors. The calculated bioactivity scores for GSH monomer and dimer species are presented in Table 2.

Organic molecules are categorized as biologically active when bioactivity scores are higher than zero, moderately active when the scores are between −5.0 and zero and inactive when the bioactivity score lies below −5.0. From the values of the bioactivity scores reported in Table 2, it seems that both GSH monomer and dimer species are moderately bioactive with the monomer to be more active than dimer.

It is very important to assess the reactivity of compounds with biological applications. Global reactivity descriptors according to Koopmans' theorem are representative quantities for understanding the ability of molecules to interact with other molecules or biological targets [39,40]. The values of the descriptors for the glutathione monomer and dimer molecule are presented in the Table 3. These descriptors provide significant information concerning the reactivity and site selectivity of the compared GSH species.

HOMO-LUMO energy gap (ΔE) indicates the ability to excite the electrons of a molecule and is therefore related to its reactivity. Specifically, a smaller energy gap implies a reduction in its stability and an increase in its ability to interact with other molecules [41]. HOMO and LUMO diagrams for both monomer and dimer are presented in Fig. 11.

Global hardness (η) is associated with the ease of changing the electronic cloud that could be observed when two molecules interact with each other. Low values of global hardness favour this interaction and decrease the stability of the molecule [42]. High global hardness or large HOMO-LUMO energy gap (ΔE) reflects hard molecules with more rigid structure. On the contrary, global softness (s) is inversely proportional to hardness. Compounds characterized by greater values of softness also show greater polarizability, which allows them to participate

Table 1
Molecular properties of GSH monomer and dimer species. All calculations were performed online utilizing Molinspiration software (https://molinspiration.com).

Molecular properties	GSH monomer	GSH dimer
milogP	−4.97	−5.93
Total polar surface area, TPSA (Å^2)	158.82	309.80
Natoms	20	40
MW	307.33	615.66
nON	9	18
nOHNH	6	13
nviolations	1	3
Number of rotatable bonds, nrotb	9	22
volume	259.22	524.51

Table 2
Bioactivity scores for GSH monomer and dimer species. All calculations were performed online utilizing Molinspiration software (https://molinspiration.com).

Bioactive acceptors	GSH monomer	GSH dimer
GPCR ligand	0.43	0.34
Ion channel modulator	0.28	−0.12
Kinase inhibitor	−0.10	−0.11
Nuclear receptor	−0.22	−0.15
Protease inhibitor	1.13	0.69
Enzyme inhibitor	0.75	0.34

Table 3
Reactivity parameters of monomer and dimer structure of glutathione according to Koopman's theorem [39,40]. Calculations were carried out using the B3LYP/6-31G (d, p) method in vacuum.

Parameter	GSH monomer	GSH dimer
E_{HOMO} (eV)	−6.45427	−6.20229
E_{LUMO} (eV)	−0.13415	−1.21417
HOMO-LUMO energy gap $\Delta E = E_{LUMO} - E_{HOMO}$ (eV)	6.32012	4.98812
Ionization energy, $I = -E_{HOMO}$ (eV)	6.45427	6.20229
Electronic affinity, $A = -E_{LUMO}$ (eV)	0.13415	1.21417
Electronegativity, $\chi = (I + A)/2$ (eV)	3.29421	3.70823
Global hardness, $\eta = (I-A)/2$ (eV)	3.16006	2.49406
Global softness, $s = 1/2\eta$ (eV^{-1})	0.15822	0.20048
Chemical potential, $\mu = (E_{HOMO} + E_{LUMO})/2 = -\chi$ (eV)	−3.29421	−3.70823
Electrophilicity, $\omega = \mu^2/2\eta$	1.71703	2.75675

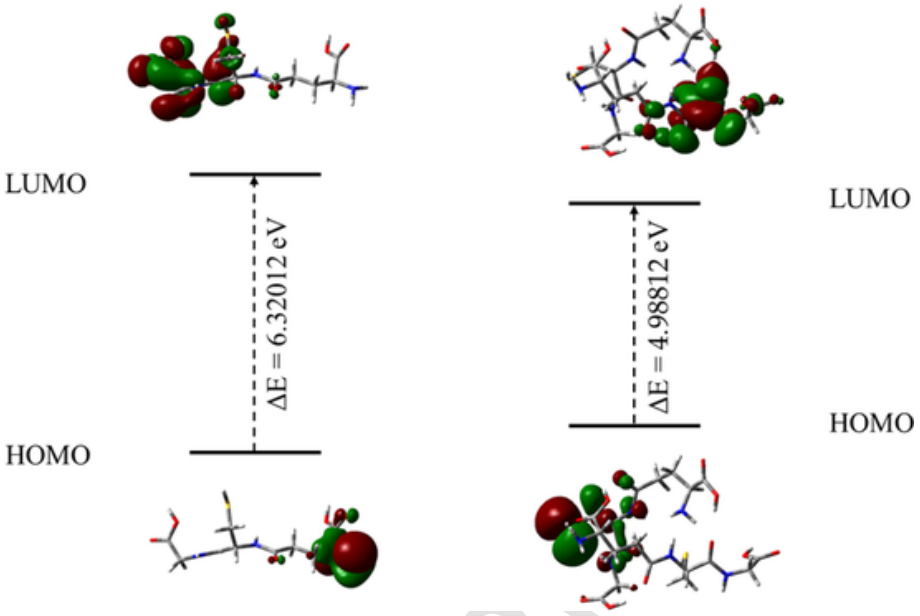

Fig. 11. HOMO and LUMO diagrams for both monomer and dimer.

more easily in chemical processes [41]. From a biological point of view, electronegativity (χ) and electrophilicity (ω) are equally important parameters. Molecules with a higher electronegativity value tend to form covalent and hydrogen bonds more easily [41]. Electrophilicity index is a measure of energy lowering caused by the high electron flow among donor and acceptor. Furthermore, electronic charge exchange with biological molecules is favoured in molecules with a high electrophilicity value, as they could accept a pair of electrons [42]. With chemical potential (μ) we define the escaping tendency of the electrons from a stable molecule. Negative values of chemical potential indicate that the system is stable, and it does not decompose in spontaneous manner into its elements [42]. It seems that both GSH monomer and dimer possess negative chemical potential. High ionization potential (I) indicates improved potential to interact with heavy metal atoms. Finally, increased electron affinity (A) reveals the ability of a molecule to accept one electron from a donor.

Based on the above discussion and the values of the descriptors presented in the Table 3, the conclusion reached is that the dimer of glutathione is characterized by less stability, greater reactivity, and greater tendency to interact with biological compounds. Furthermore, it is widely accepted that liver plays a crucial role in carrying out a variety of essential biological processes, such as detoxification and protein synthesis. Within the liver, glutathione is normally present in the liver at a concentration of 10 mM [43]. The structure of GSH at this concentration levels is mainly composed of dimers preventing further the formation of intermolecular interactions that create hydrogen bonds. As a result, proteins can connect through thiol groups and form disulfide bonds, which provide more stability.

4. Conclusions

In the present work, we combined concentration-dependent ultrasonically induced birefringence measurements with molecular docking and DFT methodologies to study the dynamic response of glutathione in aqueous environment. Birefringence signals are attributed to the orientation of molecular moieties in the direction of the applied ultrasonic field.

Molecular docking study revealed the presence of a dimerization scheme, and the corresponding binding free energy was estimated equal to −3.44 kcal/mol. The interaction between the two monomeric units constituting the dimer is mostly hydrogen bonding. The formation of higher aggregates, such as trimers, tetramers, etc. is not expected to occur in the concentration region studied here. The oxidation of GSH to GSSG is the basis of all major intercellular reactions in-volving GSH. However, this phenomenon cannot be observed in aqueous solutions unless an oxidizing agent is present.

The maximum birefringence values in the stationary region experience a drastic change when approaching the concentration C = 4 mM instead of a rather monotonic trend with increasing concentration. This behavior is attributed to the dimerization reaction occurring in the aqueous GSH solutions.

Moreover, several physical properties, including mass density, shear viscosity, sound speed, isentropic compressibility, specific conductivity, and pH were also measured as function of solution concentration and all exhibit a sudden change near 4 mM, which is indicative of the gradual aggregation process occurring in the aqueous GSH solutions.

The volume ratio between dimer and monomer was found experimentally equal to 1.62 for concentration 10 mM and estimated theoretically by means of PM6 semi-empirical method equal to 1.95. It seems that dimers dominate the structure of GSH aqueous solutions in the relatively dilute region. The deviation between the two values can be understood if we consider that the molecular docking and PM6 semi-empirical methods were performed in a vacuum environment.

The chemical reactivity and the biological activity of the GSH monomer and dimer species were evaluated and compared revealing that the dimer species of glutathione is characterized by less stability, greater reactivity, and greater tendency than monomer to interact with biological compounds.

Funding

This research did not receive any specific grant from funding agencies in the public, commercial, or not-for-profit sectors.

CRediT authorship contribution statement

A. Tryfon : Investigation. **P. Siafarika :** Investigation. **C. Kouderis :** Investigation. **A.G. Kalampounias :** Conceptualization, Investigation, Methodology, Supervision, Validation, Writing – original draft, Writing – review & editing.

Declaration of Competing Interest

The authors declare that they have no known competing financial interests or personal relationships that could have appeared to influence the work reported in this paper.

Data availability

Data will be made available on request.

Acknowledgments

P. Siafarika acknowledges support by project "Dioni: Computing Infrastructure for Big-Data Processing and Analysis." (MIS No. 5047222) which is implemented under the Action "Reinforcement of the Research and Innovation Infrastructure", funded by the Operational Programm "Competitiveness, Entrepreneurship and Innovation" (NSRF 2014-2020) and co-financed by Greece and the European Union (European Regional Development Fund)."

References

[1] A.K. Tummanapelli, S. Vasudevan, Ab initio MD simulations of the Brønsted acidity of glutathione in aqueous solutions: predicting pKa shifts of the cysteine residue, J. Phys. Chem. B 119 (2015) 15353.
[2] M. Picquart, L. Grajcar, M.H. Baron, Z. Abedinzadeh, Vibrational spectroscopic study of glutathione complexation in aqueous solutions, Biospectroscopy 5 (1999) 328.
[3] A. Krezel, W. Bal, Coordination chemistry of glutathione, Acta Biochim. Pol. 46 (1999) 567.
[4] E. Valencia, A. Marin, G. Hardy, Glutathione-nutritional and pharmacological viewpoints: part II, Nutrition 17 (2001) 485.
[5] G. Wu, Y. Fang, S. Yang, J.R. Lupton, N.D. Turner, Glutathione metabolism and its implications for health, J. Nutr. 134 (2004) 489.
[6] H.J. Forman, H. Zhang, A. Rinna, Glutathione: overview of its protective roles, measurement, and biosynthesis, Mol. Aspects Med. 30 (2009) 1.
[7] J.C. Cameron, H.B. Pakrasi, Glutathione facilitates antibiotic resistance and photosystem I stability during exposure to gentamicin in cyanobacteria, Appl. Environ. Microbiol. 77 (2011) 3547.
[8] A.L. Turnbull, M.G. Surette, Cysteine biosynthesis, oxidative stress and antibiotic resistance in *Salmonella typhimurium*, Res. Microbiol. 161 (2010) 643.
[9] J. Pizzorno, Glutathione!, Integr. Med. (Encinitas) 13 (2014) 8.
[10] J.W. Finley, A.N. Kong, K.J. Hintze, E.H. Jeffery, L.L. Ji, X.G. Lei, Antioxidants in foods: state of the science importance to the food industry, J. Agric. Food Chem. 59 (2011) 6837.
[11] M. Risva, S. Tsigoias, S. Boghosian, S. Kaziannis, A.G. Kalampounias, Exploring the influence of urea on the proton-transfer reaction in aqueous amine solutions with Raman and ultrasonic relaxation spectroscopy, Mol. Phys. 121 (2023) e2163314.
[12] A.G. Kalampounias, Establishing the role of shear viscosity on the rate constants of conformational fluctuations in unsaturated aldehydes, Chem. Phys. 561 (2022) 111618.
[13] H. Nomura, T. Matsuoka, S. Koda, Translational-orientational coupling motion of molecules in liquids and solutions, J. Mol. Liq. 96–97 (2002) 135–151.
[14] X. Xiong, A. Busnaina, S. Selvarasah, S. Somu, M. Wei, J. Mead, C. Chen, J. Aceros, P. Makaram, M.R. Dokmeci, Directed assembly of gold nanoparticle nanowires and networks for nanodevices, Appl. Phys. Lett. 91 (2007) 063101.
[15] W. Zhang, L. Huang, C. Santschi, O.J. Martin, Trapping and sensing 10 nm metal nanoparticles using plasmonic dipole antennas, Nano Lett. 10 (2010) 1006–1011.
[16] L.T. Cai, H. Skulason, J.G. Kushmerick, S.K. Pollack, J. Naciri, R. Shashidhar, D.L. Allara, T.E. Mallouk, T.S. Mayer, Nanowire-based molecular monolayer junctions: synthesis, assembly, and electrical characterization, J. Phys. Chem. B 108 (2004) 2827–2832.
[17] R. Stevens, L. Stevens, N.C. Price, The stabilities of various thiol compounds used in protein purifications, Biochem. Educ. 11 (1983) 70.
[18] P. Siafarika, M.G. Papanikolaou, T.A. Kabanos, A.G. Kalampounias, Probing the equilibrium between mono- and di-nuclear nickel(II)-diamidate [NiII(DQPD)]x, x = 1,2 complexes in chloroform solutions by combining acoustic and vibrational spectroscopies and molecular orbital calculations, Chem. Phys. 549 (2021) 111279.
[19] C. Kouderis, P. Siafarika, A.G. Kalampounias, Disentangling proton-transfer and segmental motion relaxations in poly-vinylalcohol aqueous solutions by means of ultrasonic relaxation spectroscopy, Polymer 217 (2021) 123479.
[20] A.G. Kalampounias, Exploring conformational change profile of n-propyl ester of formic acid by combining ultrasonic relaxation spectroscopy and molecular orbital calculations, J. Mol. Struct. 1212 (2020) 128146.
[21] G. Stogiannidis, S. Tsigoias, A.G. Kalampounias, Conformational energy barriers in methyl acetate – Ethanol solutions: a temperature-dependent ultrasonic relaxation study and molecular orbital calculations, J. Molec. Liq. 302 (2020) 112519.
[22] A. Tryfon, P. Siafarika, C. Kouderis, S. Kaziannis, S. Boghosian, A.G. Kalampounias, Evidence of self-association and conformational change in Nisin antimicrobial polypeptide solutions: a combined Raman and ultrasonic relaxation spectroscopic and theoretical study, Antibiotics 12 (2023) 221.
[23] C. Kouderis, S. Tsigoias, P. Siafarika, A.G. Kalampounias, The effect of alkali iodide salts in the inclusion process of phenolphthalein in β-cyclodextrin: a spectroscopic and theoretical study, Molecules 28 (2023) 1147.
[24] A.D. Becke, Density-functional thermochemistry. III., The role of exact exchange, J. Chem. Phys. 98 (1993) 5648.
[25] C. Lee, W. Yang, R.G. Parr, Development of the Colle-Salvetti correlation-energy formula into a functional of the electron density, Phys. Rev. B 37 (1988) 785.
[26] S. Fujiwara, G. Formicka-Koziowska, H. Kozlowski, Conformational study of glutathione by NMR, Bull. Chem. Soc. Jap. 50 (1977) 3131–3135.
[27] O. Lampela, A.H. Juffer, A. Rauk, Conformational analysis of glutathione in aqueous solution with molecular dynamics, Chem. A Eur. J. 107 (2003) 9208–9220.
[28] M.E. Cromwell, E. Hilario, F. Jacobson, Protein aggregation and bioprocessing, AAPS J. 8 (2006) E572–E579.
[29] K. Engelhardt, M. Lexis, G. Gochev, C. Konnerth, R. Miller, N. Willenbacher, W. Peukert, B. Braunschweig, pH effects on the molecular structure of β-lactoglobulin modified air–water interfaces and its impact on foam rheology, Langmuir 29 (2013) 11646–11655.
[30] E.Y. Chi, S. Krishnan, T.W. Randolph, J.F. Carpenter, Physical stability of proteins in aqueous solution: mechanism and driving forces in nonnative protein aggregation, Pharm. Res. 20 (2003) 1325–1336.
[31] N.W. Pirie, K.G. Pinhey, The titration of glutathione, J. Biol. Chem. 84 (1929) 321–333.
[32] A. Meretoudi, C.N. Banti, P. Siafarika, A.G. Kalampounias, S.K. Hadjikakou, Tetracycline-water soluble formulations with enhanced antimicrobial activity, Antibiotics 9 (2020) 845.
[33] M. Matsumoto, H. Watanabe, K. Yoshioka, A method for determining the relaxation spectrum from the decay curve of electric birefringence of macromolecular solutions, Kolloid Z. Z. Polym. 250 (1972) 298–302.
[34] G. Stogiannidis, S. Tsigoias, S. Kaziannis, A.G. Kalampounias, Stationary and transient acoustically induced birefringence of methyl acetate molecules dissolved in ethanol, Chem. Pap. 74 (2020) 2059–2067.
[35] C. Kouderis, S. Tsigoias, P. Siafarika, A.G. Kalampounias, Acoustically induced birefringence in polymer aqueous solutions: the case of polyvinyl alcohol, Phys. B 643 (2022) 414189.
[36] C. Kouderis, A.G. Kalampounias, Combined use of ultrasonic and electromagnetic fields for the study of bonding mechanisms between dexamethasone disodium phosphate molecules, Quantum Beam Sci. 7 (2023) 19.
[37] C.A. Lipinski, F. Lombardo, B.W. Dominy, P.J. Feeney, Experimental and computational approaches to estimate solubility and permeability in drug discovery and development settings, Adv. Drug Deliv. Rev. 46 (2001) 3–26.
[38] P. Leeson, Drug discovery: chemical beauty contest, Nature 481 (2012) 455–456.
[39] P. Geerling, F. De Proft, W. Langenaeker, Conceptual density functional theory, Chem. Rev. 103 (2003) 1793.
[40] D. Glossman-Mitnik, Computational study of the chemical reactivity properties of the rhodamine B molecule, Procedia Comput. Sci. 18 (2013) 816.
[41] S. Janeoo, S. Reenu, A. Saroa, R. Kumar, H. Kaur, Computational investigation of bioactive 2,3-diaryl quinolines using DFT method: FT- IR, NMR spectra, NBO, NLO, HOMO-LUMO transitions, and quantum-chemical properties, J. Molec. Struct. 1253 (2022) 132285.
[42] V.K. Choudhary, A.K. Bhatt, D. Dash, N. Sharma, DFT calculations on molecular structures, HOMO-LUMO study, reactivity descriptors and spectral analyses of newly synthesized diorganotin (IV) 2-chloridophenylacetohydroxamate complexes, J. Comput. Chem. 40 (2019) 2354.
[43] S.C. Gad, Glutathione, in: P. Wexler (Ed.), Encyclopedia of Toxicology, 3rd ed., Elsevier, Academic Press, 2014, p. 751.